CHEMISTRY OF MATERIALS

Article

pubs.acs.org/cm

Spatially Resolved, Site-Dependent Charge Transfer and Induced Magnetic Moment in TCNQ Adsorbed on Graphene

Davide Maccariello,[†,‡] Manuela Garnica,[†,‡] Miguel A. Niño,[†] Cristina Navío,[†] Paolo Perna,[†] Sara Barja,[†,‡] Amadeo L. Vázquez de Parga,[†,‡] and Rodolfo Miranda*[,†,‡]

[†]Instituto Madrileño de Estudios Avanzados en Nanociencia (IMDEA-Nanociencia), Cantoblanco, 28049 Madrid, Madrid, Spain

[‡]Departamento Física de la Materia Condensada, Universidad Autónoma de Madrid, Cantoblanco, 28049 Madrid, Madrid, Spain

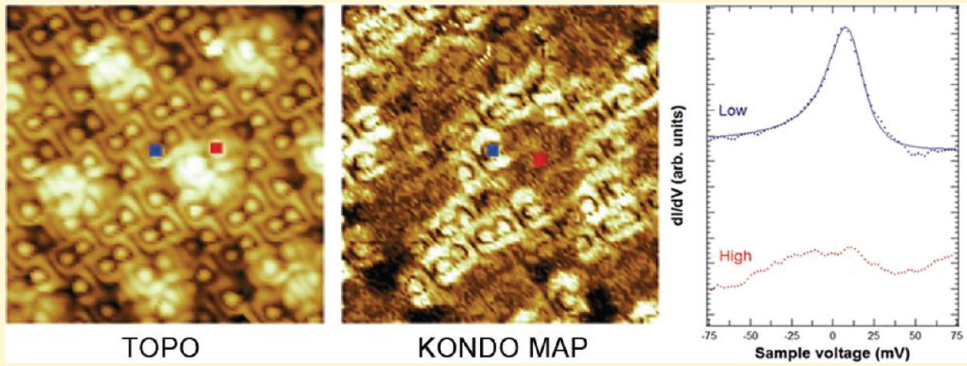

ABSTRACT: A site-dependent charge transfer to 7,7′,8,8′-tetracyanoquinodimethane (TCNQ) adsorbed on a single layer of periodically rippled graphene grown epitaxially on Ru(0001), identified by X-ray photoemission techniques, can be spatially resolved using Scanning Tunneling Microscopy, which can also detect the formation of magnetic moments. The molecules adsorbed on the lower part of the ripples are charged with electrons donated from the doped graphene overlayer and develop a magnetic moment, while those at the upper part of the ripples are neutral. On the other hand, TCNQ adsorbed on graphene on Ir(111) shows negligible charge transfer and no magnetic moment. These observations explain the spatially dependent long-range magnetic order observed recently for TCNQ on gr/Ru(0001).

INTRODUCTION

The production of ordered arrays of magnetic objects in two dimensions is a topic that has attracted sustained interest for years.[1] While this has been achieved by nanolithographic means for metallic objects with diameters of the order of tens of nanometers,[2] the ultimate limit of miniaturization (and identical size) of the magnetic objects imply the use of magnetic molecules and their self-organization on surfaces.[3] The goal is to achieve a long-range structural ordering of magnetic molecules in two dimensions and, possibly, their long-range magnetic ordering due to mutual interactions between these molecules. Many molecules that show magnetic moment in the gas phase have been deposited on (mostly metal) surfaces, where the interaction with the substrate often eliminate the magnetic moment[4] and always complicate their mutual interaction by keeping the magnetic centers too far away. Another approach follows from the discovery of magnetic order in organic charge transfer compounds. Since the introduction of the first organic-based magnet, e.g. $[FeII(C_5Me_5)_2]^{\bullet+}$ $[TCNE]^{\bullet-}$ (decamethylferrocene alternating with tetracyanoethenide (TCNE)) with a low critical temperature (Tc = 4.8 K),[5] metal−organic bulk magnets consisting of strong electron acceptors, such as TCNE or 7,7′,8,8′-tetracyanoquinodimethane (TCNQ) and metal atoms (V, Fe, etc.) that donate them electrons have been intensively studied,[6] with some of them showing long-range magnetic order with critical temperatures above 300 K.[7,8] This type of compound is based on charge transfer between their components, but so far it always requires the presence of metal ions. Recently, however, long-range magnetic order in a purely organic 2D material has been reported.[9] The material consists of a full monolayer of TCNQ adsorbed on a heavily n-doped graphene monolayer grown on Ru(0001).[10] The electrons donated by the graphene layer to the TCNQ molecules populate a spin-split intermolecular band, their exchange interaction resulting in long-range magnetic order at 4.6 K.[9] This result is a prominent example of a much explored strategy to modify graphene properties, specifically to add magnetic functionalities to graphene-based heterostructures by depositing and self-organizing organic molecules on epitaxial graphene.

The complex magnetic order visualized by spin-polarized Scanning Tunneling Microscopy (STM)[9] for TCNQ on graphene/Ru(0001) is a consequence of the prediction of different magnetic moments for TCNQ molecules adsorbed on

Received: February 14, 2014
Revised: March 19, 2014

 © XXXX American Chemical Society dx.doi.org/10.1021/cm5005467 | Chem. Mater. XXXX, XXX, XXX−XXX

different locations of the periodically corrugated graphene/Ru(0001) substrate,[9] related to a different degree of charge transfer. This theoretical prediction calls for an experimental characterization of the site-dependent charge transfer in this system by a suitable combination of experimental techniques. We report here on the charge transfer between TCNQ and different adsorption sites on single layers of graphene epitaxially grown on Ru(0001) and Ir(111) single-crystal surfaces by X-ray Photoelectron Spectroscopy (XPS), STM, Scanning Tunneling Spectroscopy (STS), and Ultraviolet Photoelectron Spectroscopy (UPS). For gr/Ru(0001), we find that the molecules adsorbed on the lower parts of the ripples ("valleys") are charged, while those adsorbed on the upper part of the ripples ("hills") are not. The TCNQ molecules are essentially neutral when adsorbed on the lightly p-doped graphene/Ir(111) substrate. The lack of magnetic moment for the adsorbed TCNQ molecules in the latter case confirms the importance of the charge transfer from gr/Ru(0001) for the electron population of the intermolecular bands in order to achieve long-range magnetic order[9] in these purely organic 2D materials.

RESULTS AND DISCUSSION

Graphene on Ir(111) and Ru(0001). Graphene can be epitaxially grown on Ir(111)[11,12] and Ru(0001)[10,13−15] by thermal decomposition of ethylene at 1250 K. The moiré pattern of gr/Ir(111) shows a 2.52 nm periodic arrangement of darker regions ("holes"), 0.02 nm deep at high bias voltages,[11] which is illustrated in Figure 1a. The darker regions correspond

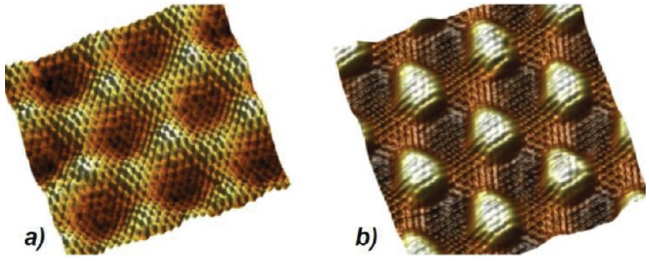

Figure 1. High resolution 3D topographic STM images of a) graphene on Ir(111) (7.4 × 6.5 nm^2, V_b = 0.3 V, I_t = 100 pA) and b) graphene on Ru(0001) (9 × 9 nm^2, V_b = −5 mV, I_t = 100 pA).

to the "atop" areas, where the C honeycomb of graphene is centered on an Ir atom. The monolayer graphene is perfectly aligned with the high symmetry direction of the Ir substrate resulting in a 9.32 × 9.32 incommensurate superstructure.[11] The C−Ir vertical distance is relatively large (0.34 nm) indicating a week bonding to the metal. The epitaxial monolayer on graphene on Ir(111) is slightly p-doped (each C atom has lost ∼0.01 electrons to the substrate) with the Dirac energy 100 meV above the Fermi level.[12] In spite of the weak structural corrugation the electronic structure of gr/Ir(111) is rather homogeneous spatially, as indicated by the observation of a unique set of Field Emission Resonances[16] and the lack of changes in the apparent corrugation with the bias voltage. The moiré structure for graphene on Ru(0001) shows a self-organized array of hills (H) and valleys (L), with an apparent height of 0.1 nm and a lateral periodicity of 3 nm, as shown in Figure 1b. The darkest regions in the valleys of the image correspond to the fcc-top sites, where three C atoms sit on the fcc interstitial sites and three directly on top of Ru atoms. Graphene strongly interacts with Ru(0001), and, as a result, it is n-doped with substantial charge transfer from the Ru substrate.[10] The electronic structure of this periodically rippled graphene layer is spatially heterogeneous, with certain electronic states localized on the hills,[17,19] a larger conductance at the Fermi level on the hills,[10] and a smaller surface potential,[17] larger electron density, and larger electron−phonon coupling at the valleys.[20]

Neutral TCNQ on Graphene/Ir(111). Unlike gr/Ru(0001) (see below), the graphene layers grown on Ir(111) do not present preferential adsorption sites for TCNQ molecules. Figure 2 shows representative STM images of the

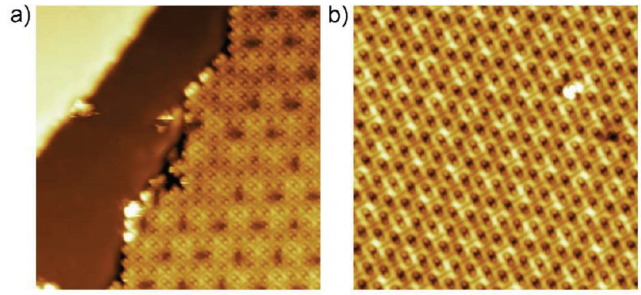

Figure 2. STM images recorded at 4.6 K of a) the edge of an island of TCNQ on gr/Ir(111) 20 × 20 nm^2, V_s = 1 V, I_t = 50 pA and b) a complete monolayer of TCNQ on gr/Ir(111) (15 × 15 nm^2) recorded with V_s = 1 V and I_t = 40 pA.

growth of the TCNQ monolayer. Islands with compact shape appear upon deposition at 300 K and imaging at 4.6 K, indicating that the net intermolecular interaction is attractive.

Upon increasing the coverage, a complete ML of TCNQ with a square lattice similar to the one of the bulk is obtained. The closed packed structure is stabilized via strong C≡N···H−C hydrogen bonds between the cyano groups and the hydrogens in the central ring. The $\pi-\pi^*$ interaction binds the molecule to the substrate.[21] Similar independence of the substrate symmetry has been reported for the self-organized adsorption of Cobalt Phthalocyanine (CoPc) on gr/Ir(111).[22]

The XPS signal coming from the N1s level is clearly visible already at submonolayer coverage of TCNQ (Figure 3). The signal increases with increasing coverage and reaches saturation near completion of the ML. At 300 K only the first ML is stable on gr/Ir(111). The N1s line shape can be fitted with only one component with a fwhm of 0.9 eV at a Binding Energy (BE) of 399.3 eV, plus a shakeup satellite at 401.9 eV. The shakeup satellite results from an intermolecular excitation process, by which the emission of the 1s electron is accompanied by an electronic excitation from the HOMO to the LUMO level. The difference in energy between the shakeup peak and the main N1s core level (2.6 eV) is, thus, related to the HOMO−LUMO energy difference. The observed N1s core level corresponds to a TCNQ molecule with negligible charge, i.e. neutral (N^0), in agreement with the N1s values reported for neutral TCNQ,[23−25] i.e. 399.5 eV (and 402.1 eV for its shake up satellite). The N1s core level of the neutral species of F4-TCNQ adsorbed on graphene (SiC) has also been observed at a similar BE of 399.6 eV.[26]

For clean graphene/Ir(111), a single XPS C1s core level corresponding to the C atoms of the graphene layer can be clearly observed (Figure 4) at an energy of 284.2 eV, in agreement with previous reports.[27] The proximity of the Ir

dx.doi.org/10.1021/cm5005467 | Chem. Mater. XXXX, XXX, XXX−XXX

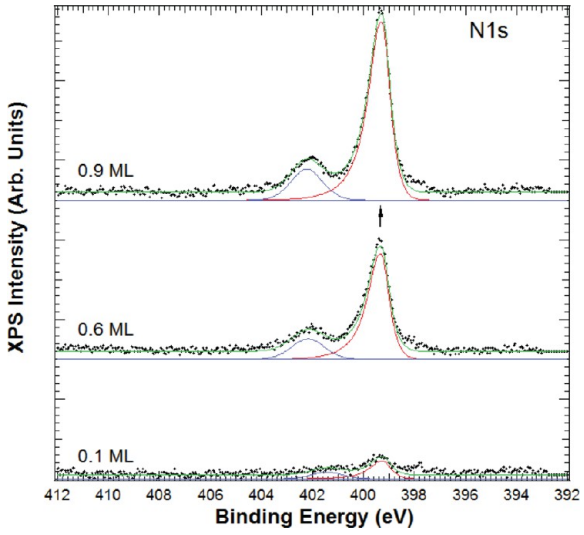

Figure 3. Selected XPS N1s core level spectra for increasing amounts of TCNQ deposited at 300 K on graphene/Ir(111). The red line corresponds to the N1s component and the blue line to the shake up. The green line is the corresponding sum of components.

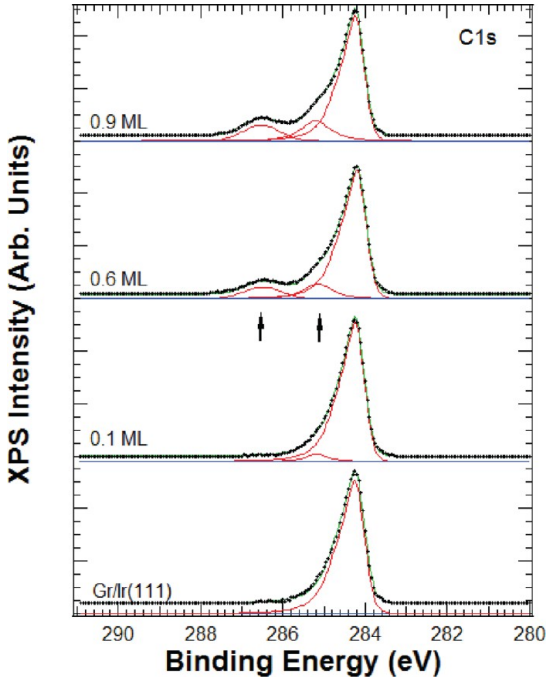

Figure 4. XPS C1s core level spectra for gr/Ir(111) and increasing amounts of TCNQ deposited at 300 K on it. The fits to the different components (the arrows signal the ones associated to TCNQ) are shown as continuous red lines. The green line is the sum of components.

4d5/2 and 4d3/2 levels (close to a BE of 300 eV) jeopardizes in our case the observation of the carbon plasmon and the adequate background subtraction. Upon deposition of TCNQ, two components corresponding to the carbon atoms of the TCNQ molecules (in addition to the C1s level of the graphene/Ir(111) substrate) appear at 285.2 eV (quinone group) and 286.5 eV (cyano ring), respectively, as shown in Figure 4. These values are identical to the ones reported for neutral TCNQ powder,[23,24] confirming that TCNQ adsorbed on gr/Ir(111) is in a neutral state. The corresponding C1s core levels for cyano groups and quinone ring in (partly) anionic TCNQ adsorbed on Cu(100) appear indeed shifted to lower BEs, i.e, at 284.6 and 285.7, respectively.[25] The relative areas of the C1s core levels, corresponding to C atoms in graphene and C atoms in TCNQ, correlate nicely with the respective atomic densities deduced from the STM images shown above, i.e. 2.86 $\times$ 10^{15} C at/cm^2 for graphene and 1.34 $\times$ 10^{15} C at/cm^2 for TCNQ, respectively.

Figure 5 shows a series of UPS spectra recorded for increasing coverage of TCNQ on gr/Ir(111) plus the one

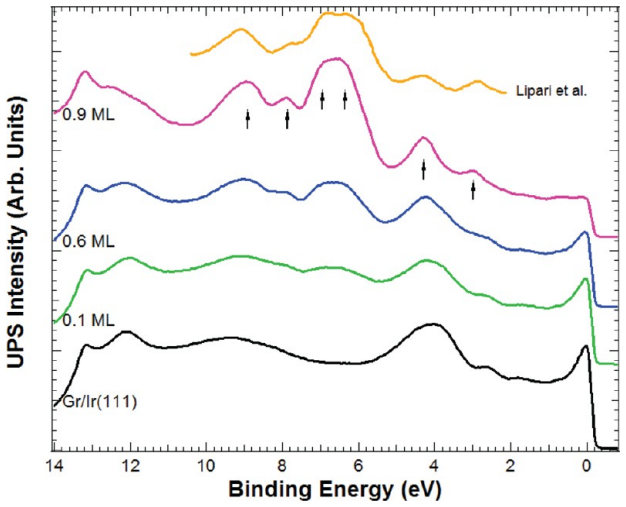

Figure 5. UPS spectra of the valence band recorded using hν = 21.2 eV at 35° emission for increasing amounts of TCNQ deposited at 300 K on graphene/Ir(111).The arrows indicate the valence band levels of adsorbed TCNQ. The upper spectrum, taken from ref 29, corresponds to bulk (neutral) TCNQ.

corresponding to bulk, neutral TCNQ (above). The lower spectrum corresponds to gr/Ir(111). Upon deposition, five peaks (one of them double) reflecting the occupied valence levels of TCNQ molecules at 3.0, 4.3, 6.3−7.0, 7.8, and 9.0 eV below the Fermi energy are clearly detected. It is remarkable that already at submonolayer coverage the valence band looks very similar in energy positions and shape to the one of a TCNQ ML (and a thick neutral layer[28−30]). This indicates that the spectra are dominated by the intramolecular electronic structure of neutral molecules, unperturbed by the adsorption on gr/Ir(111). According to solid phase measurements,[28,29] the first band below the Fermi level at 3.0 eV is the highest occupied molecular orbital (HOMO), and it has π character. There is agreement in the literature[28−30] that the HOMO level in neutral TCNQ adsorbed on a number of substrates is located at 3.0 eV below the Fermi level.

The second band at 4.3 eV, with π character too, is essentially localized in the carbon ring, probably with some σ character. The broad (double-peaked) third band is assigned to orbitals localized in the CN groups, corresponding to three lone pairs of the nitrogen atom and two different π orbitals. The fourth and fifth bands have mainly σ character.[28,29] All the peaks observed for TCNQ on gr/Ir(111) coincide within 0.1 eV with the (rigidly shifted) gas phase values and the values obtained for thick TCNQ films.[28−30] This confirms that TCNQ molecules adsorbed on gr/Ir(111) are not charged. The similarity in line shape for the adsorbed ML and the bulk samples further

dx.doi.org/10.1021/cm5005467 | Chem. Mater. XXXX, XXX, XXX−XXX

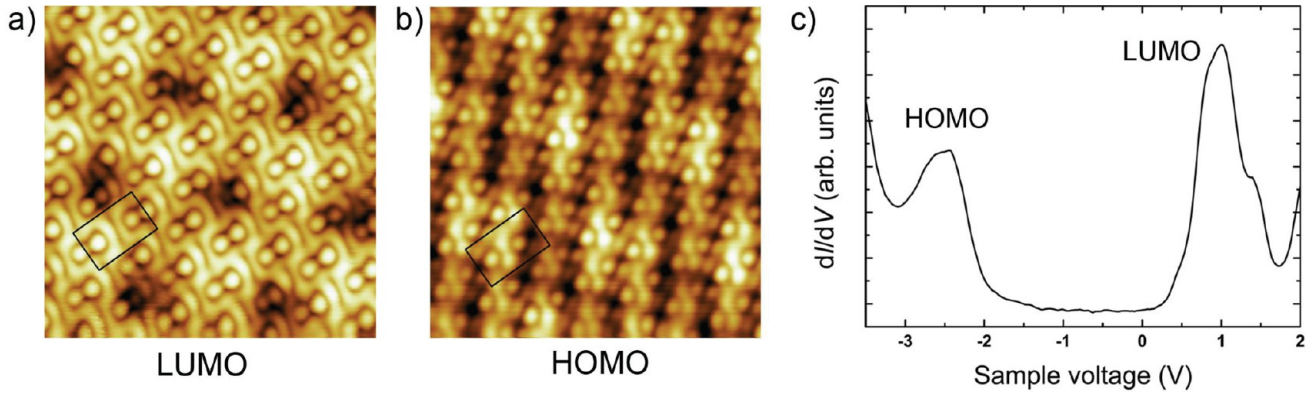

Figure 6. STM topographic images (7×7 nm^2) of a ML of TCNQ on gr/Ir(111) recorded at energies corresponding respectively to a) the LUMO orbital at +1 V, I = 50 pA and b) the HOMO level at V_s = −2.5 V, I = 50 pA; and c) STS spectrum for TCNQ adsorbed on graphene/Ir(111) recorded with the tunneling gap stabilized at V_s = 2 V and I = 40 pA.

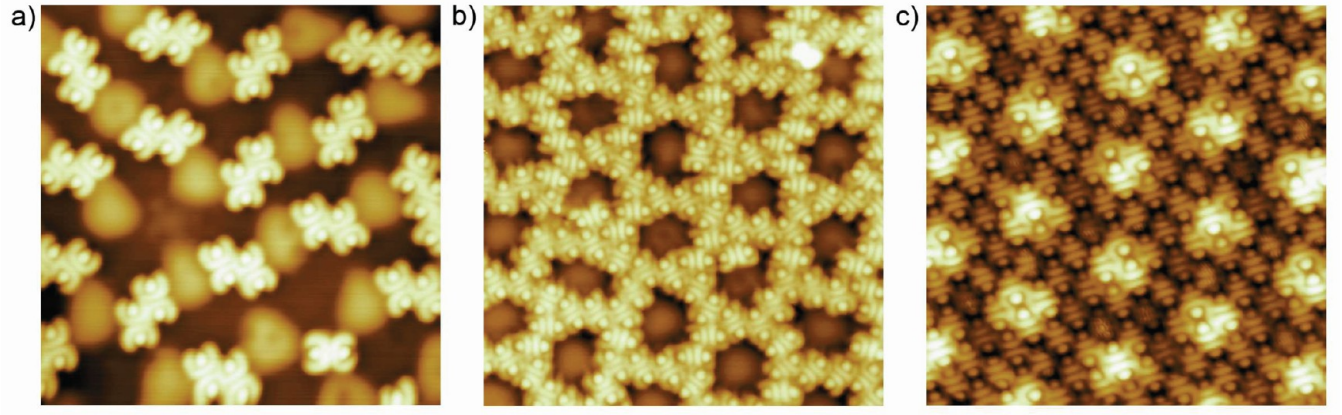

Figure 7. STM topographic images (12 nm × 12 nm) of TCNQ/graphene/Ru(0001) at different coverage: a) 0.3 ML, isolated molecules, dimers and trimers at the early stages of the deposition, acquired with V_s = 1 V and I_t = 10 pA; b) 0.6 ML, a highly ordered, self-organized arrangement of TCNQ molecules selectively adsorbed on the lower parts of the ripples, acquired with V_s = −1 V and I_t = 50 pA; and c) a complete monolayer of TCNQ acquired with V_s = 2 V and I_t = 100 pA. The brighter molecules are the ones adsorbed on the upper parts of the ripples.

indicates that the TCNQ orbitals are efficiently decoupled from the metallic substrate by the monolayer of graphene.

Figure 6 shows high resolution STM topographic images corresponding to the occupied HOMO state and the empty LUMO state of TCNQ/gr/Ir(111) as detected by STS (see below). At ML completion, the TCNQ molecules self-assemble in a compact arrangement forming rows arranged along their long axes, with molecules in adjacent rows displaced with respect to each other (originating a rhombic symmetry).[21] Local Scanning Tunnel Spectroscopy (STS) performed with the STM on top of a TCNQ molecule adsorbed on gr/Ir(111) indicates the presence of the occupied HOMO level at −2.5 eV and the empty LUMO level at +1 eV above the Fermi level regardless of the relative adsorption, as shown in Figure 6c. The unoccupied, π^* LUMO state of neutral TCNQ powder has been detected by Inverse Photoemission at +1.8 eV.[31] From the data described above, the binding energy of the HOMO level in STS is found to be slightly smaller than in UPS (as well as the HOMO−LUMO gap). It has to be noted that STS and UPS probe different electronic states. While STS probes the ground state HOMO via resonant tunneling from the HOMO into tip empty states at the Fermi level, UPS measures an ionic (N-1 electrons) state screened by the surroundings, i.e. the polarization energy is absent in STS. The Coulomb attraction acting on the outgoing photoelectrons reduces their kinetic energy, thereby increasing their apparent binding energies (BE). Thus, apparent BEs in UPS are somewhat larger than in STS.[30] We conclude that the level detected at 3.0 eV in UPS is the same HOMO level that is detected at −2.5 eV in STS, and the level detected by STS at +1 eV is assigned to the LUMO orbital of the uncharged molecule. This is similar to the values reported by STS for neutral TCNQ/Au(111), i.e. +0.7 eV.[32] In this case the weak bonding of the molecule to the Au substrate prevents an appreciable charge transfer to the molecule. In summary, all the data are consistent with the lack of charge transfer from graphene/Ir(111) to TCNQ, i.e. the adsorbed molecule is neutral in this case. A negligible (10^{-3} electrons/molecule) charge transfer has been also found for FePc adsorbed on gr/Ir(111).[33]

Charged and Neutral TCNQ on Graphene/Ru(0001). The initial deposition of TCNQ on gr/Ru(0001) produces an ensemble of isolated molecules, together with the formation of dimers, trimers and, even, pentamers. As shown in Figure 7a, for a TCNQ coverage of 0.3 ML, i.e. a density of 3.68×10^{13} molecules/cm^2, the molecules adsorb initially always on the lower part ("valleys") of the ripples, where the surface potential is lower.[17] Several phthalocyanine molecules (FePc,[34] MnPc, NiPc, H2Pc[35]) and fullerenes[36] (C_{60}) show a similar initial adsorption behavior when deposited on gr/Ru(0001). Nothing has been reported concerning the experimentally observed state

dx.doi.org/10.1021/cm5005467 | Chem. Mater. XXXX, XXX, XXX−XXX

of charge of these molecules. Each TCNQ molecule adsorbed on gr/Ru(0001), however, has been predicted to acquire a noticeable amount of charge, almost exactly 1 electron per molecule,[9] from the strongly n-doped graphene monolayer. The calculated adsorption energy for isolated TCNQ molecules (in the valley region) depends slightly on the specific adsorption geometry, ranging from 2.37 to 2.53 eV/molecule.[9]

Upon further deposition, the TCNQ molecules fully occupy the lower parts of the ripples forming a self-organized porous molecular array with coverage of 0.6 ML, i.e. a density of 6.8×10^{13} molecules/cm^2, shown in Figure 7b. The nanostructured nature of the gr/Ru(0001) substrate, thus, translates into the formation of this well ordered porous molecular structure. Most of the molecules adsorb on the bridge site between the fcc and the hcp regions of the valleys of the moiré.

An STM image of a complete ML of TCNQ deposited on gr/Ru(0001) is shown in Figure 7c, where the brighter molecules correspond to those sitting on the hills. Finally, ML completion at higher coverage forces the molecules to eventually occupy the hills of gr/Ru(0001), where the adsorption energy is, obviously, smaller than in the valleys. In fact, the average adsorption energy for the complete monolayer is reduced to 1.88 eV/molecule. At 300 K, only one monolayer of TCNQ with a density of 9.6×10^{13} molecules/cm^2 can be adsorbed on gr/Ru(0001). The STM images indicate that for a full TCNQ ML, 72.5% of the molecules occupy low (valley) sites and 27.5% the high areas.

Figure 8 shows some representative XPS N1s core levels measured during deposition of TCNQ on gr/Ru(0001). After each deposition, the gr/Ru(0001) surface was cleaned by thermal desorption of the adsorbed TCNQ (see below), and a new amount was deposited and characterized. For a coverage of 0.3 ML, the N1s core level can be fitted with a single component with a Binding Energy (BE) of 398.3 eV and a fwhm of 1 eV, which corresponds to the cyano group of the anionic species, $TCNQ^{-1}$ (N^{-1}, in the following), plus the well-known, 20% intense, shakeup satellite at 400.9 eV.[23,37] This is also in agreement with the N1s core level value (BE: 398.7 eV) reported for anionic TCNQ species on Cu(100).[25] This core level spectrum corresponds to singly negatively charged TCNQ molecules adsorbed in the lower areas of the ripples as shown in the STM image of Figure 7a.

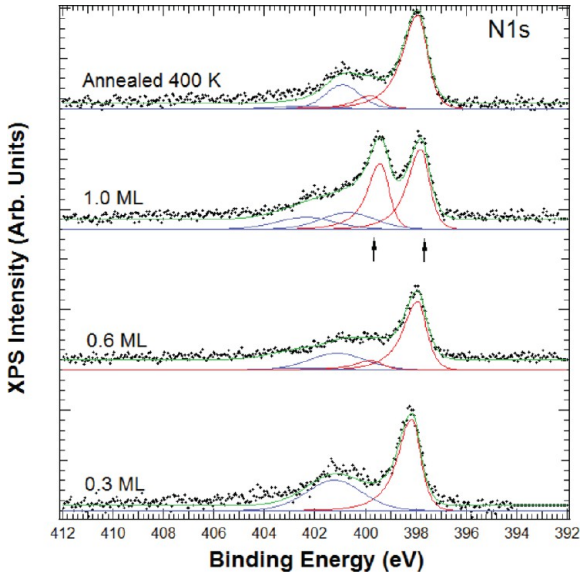

Figure 8. XPS spectra of the N1s core levels for selected coverages of TCNQ on gr/Ru(0001). The continuous red lines correspond to the fit of the two N1s components (indicated by arrows) and the blue lines to the fit of the shakeup satellites. At lower coverages one detects the "N^{-1}" ("charged") component at BE = 398.3 eV due to charge transfer to the TCNQ molecules adsorbed in the lower part of the ripples. The "N^{0}" ("neutral") component at BE = 399.5 eV is due to the TCNQ molecules in the higher part of the ripples and appears at higher coverages. Both components shift slightly to lower binding energies and saturate at 1 ML. The upper spectrum shows the almost complete disappearance of the molecules adsorbed on the upper part of the ripples as a result of annealing to 400 K.

Up to 0.6 ML only this single N1s peak is detected (although with a slight shift to a lower BE of 398.0 eV) in agreement with the STM observations (see Figure 7b) that only "low" regions of the moiré are occupied.

Above 0.6 ML, a second N1s component corresponding to the molecules that are forced to adsorb on the hills appears at higher BE (399.5 eV), with its corresponding shakeup satellite at 402.3 eV.

This second component corresponds to TCNQ molecules with negligible charge, i.e. neutral (N^0), in agreement with the N1s values reported for neutral TCNQ in bulk powders[23,24] or on gr/Ir(111) (see above), i.e. 399.5 eV for N1s and 402.1 eV for its shake up satellite.

From the annealing experiment shown in Figure 8, we estimated the site-dependent adsorption energies. In Thermal Desorption Spectroscopy (TDS) the adsorption energy, E_d, is approximately related to the temperature of the peak, T_{max}, in the desorption spectrum[38] by $E_d = k_B T_{max} [\ln(\nu T_{max}/\beta) - 3.64]$, where $\nu = 10^{13}$ s^{-1} and β is the heating rate (K·s^{-1}). The adsorption energy of TCNQ on the hills can, thus, be estimated to be of the order of 0.9 eV/molecule from the fact that annealing the sample to 400 K is enough to completely eliminate the neutral component from the N1s spectrum (see upper spectrum in Figure 8). The complete removal of the TCNQ adsorbed in the valleys requires annealing to 1000 K. Accordingly, the adsorption energy is of the order of 2.35 eV/molecule in excellent agreement with the theoretical estimation.[9]

The $TCNQ^-$ state with a −1 charge in TCNQ salts corresponds to a BE shift (with respect the neutral) of the N1s core level of 0.9 eV.[38] In our case, the core level shift is somewhat larger, 1.2 eV. From the fit we do not observe a broadening of the N^{-1} component, but a direct appearance of the N^0 component, which confirms the existence of two different kinds of adsorption sites with different charge transfer, rather than a continuous distribution of charge transfers. It has to be mentioned that during the deposition of F4-TCNQ on graphene grown on SiC, Coletti et al.[26] observed two N1s components at energies of 398.3 and 399.6 eV from the beginning. They attribute the two components to a vertical arrangement of the F4-TCNQ molecules on the graphene, in such a way that the charge transfer through the CN groups do not affect all N atoms but only those that are in contact with graphene. We do not agree with this interpretation, according also with other previous works.[40]

In addition, based on our combined STM/XPS experiments we suggest that they detected the presence of two kinds of TCNQ molecules: neutral and charged, respectively. The sequential appearance of charged and neutral TCNQ molecules is also confirmed by UPS.

dx.doi.org/10.1021/cm5005467 | Chem. Mater. XXXX, XXX, XXX−XXX

Figure 9a reproduces representative UPS spectra (recorded at 35° emission angle away from the normal) for increasing amounts of TCNQ deposited on gr/Ru(0001) at 300 K. For 0.3 ML of TCNQ five peaks (one of them double) appear. They are located at 0.85, 2.0, 3.6, 5.4−6.2, and 8.2 eV below the Fermi level. Some of them have no correspondence in the spectrum of the clean gr/Ru(0001) substrate (shown in black), while others do coincide with features in gr/Ru(0001) but can be unambiguously identified in the difference spectrum shown in Figure 9b. The observed spectrum is similar to the one of thick TCNQ, but with all the bands shifted to lower binding energy, in agreement with the substantial charge transfer to the molecule observed at this stage of the growth in the N1s core level. The intensity of this set of peaks increases with increasing coverage up 0.6 ML. They correspond to the valence band levels of charged, anionic $TCNQ^-$.[28]

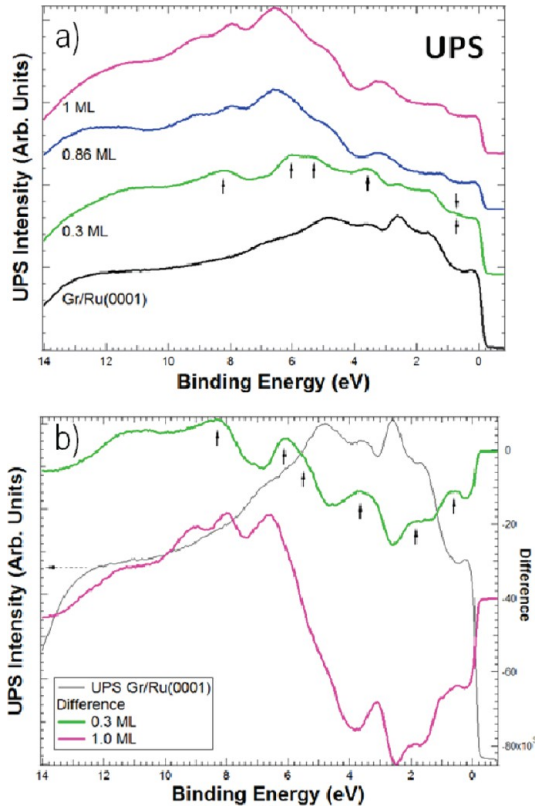

Figure 9. a) Series of UPS spectra taken using hν = 21.2 eV at 35° emission for clean gr/Ru(0001) (in black) and increasing coverages of TCNQ deposited on gr/Ru(0001) at 300 K. The arrows indicate the valence band levels of charged TCNQ; b) difference spectra corresponding to 0.3 and 1 ML, respectively. The clean gr/Ru(0001) valence band is also shown as a reference.

Above 0.6 ML a new set of peaks develops at 3.0, 4.6, 6.6, 8.0, and 9.0 eV below the Fermi level. This set is rigidly shifted ≈1 eV to higher binding energies and almost identical to the one described above for TCNQ on gr/Ir(111). It corresponds to the neutral molecules sitting on the upper part of the graphene ripples.

The closer view of the region near the Fermi edge for the UPS spectrum of TCNQ on gr/Ru(0001) shown in Figure 10a allows us to locate precisely the HOMO level. In order to see the development of a new TCNQ-related electronic state close to the Fermi edge, the curves have been normalized to the intensity of the band with a maximum at 0.2 eV (corresponding to the ruthenium 3d band states) which is attenuated with increasing TCNQ coverage. A shoulder at around 0.8 eV is indeed visible when increasing the coverage. It corresponds to the Singly Occupied Affinity Level (SOAL) that reflects the fact that the TCNQ molecules are charged with electrons coming from the doped graphene/Ru(0001) substrate. These unpaired electrons are responsible for the magnetic moment reported before for this system.[9]

The tunnelling spectrum recorded on top of TCNQ molecules adsorbed on the lower part of the ripples is shown in Figure 10b. It demonstrates the presence of the SOAL of charged TCNQ at −0.86 eV below the Fermi level, plus the doubly occupied, relaxed HOMO level at −2.0 eV (also visible in UPS). The SOAL located below the Fermi level is not doubly occupied because of a strong on-site Coulomb repulsion. For positive bias voltages the increase of differential tunnelling conductance around +1 eV is related to the presence of the LUMO.[9] Thus, an anion radical forms that has a sizable magnetic moment, as was demonstrated elsewhere[9] by detecting the corresponding Kondo resonance. Figure 10c shows the fully developed intermolecular electronic bands for a complete monolayer of TCNQ on gr/Ru(0001) with a single molecule highlighted. These bands carry the electrons donated

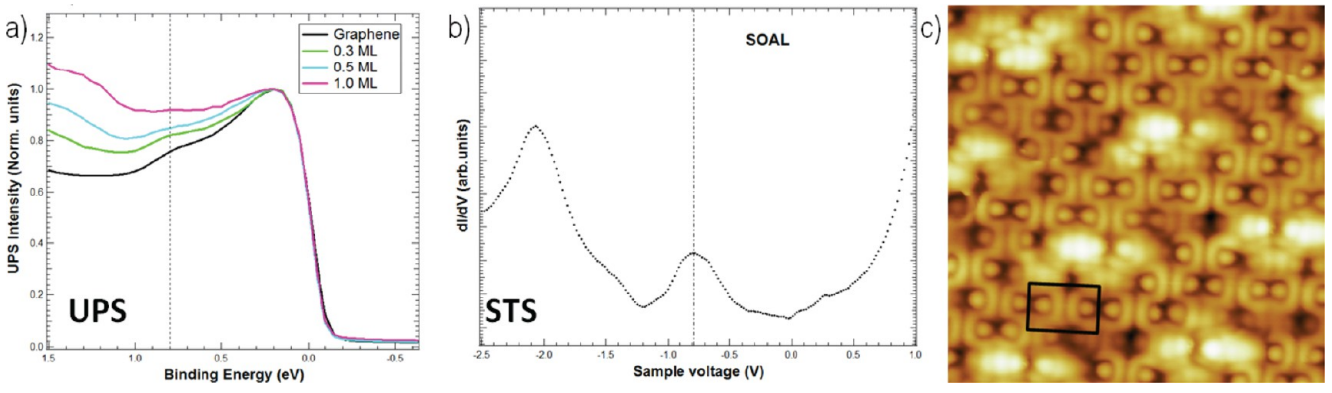

Figure 10. a) Low energy region of the UPS spectra recorded at normal emission for increasing amounts of TCNQ on gr/Ru(0001); b) Local tunnel spectroscopy recorded on top of TCNQ molecules adsorbed on gr/Ru(0001). The tunnel junction has been stabilized at a low tunneling current of 20 pA; c) Topographic STM image (7 nm × 7 nm) of a complete monolayer of TCNQ recorded with a sample voltage of −1 V and a tunnel current of 75 pA. A single molecule is highlighted by the box.

dx.doi.org/10.1021/cm5005467 | Chem. Mater. XXXX, XXX, XXX−XXX

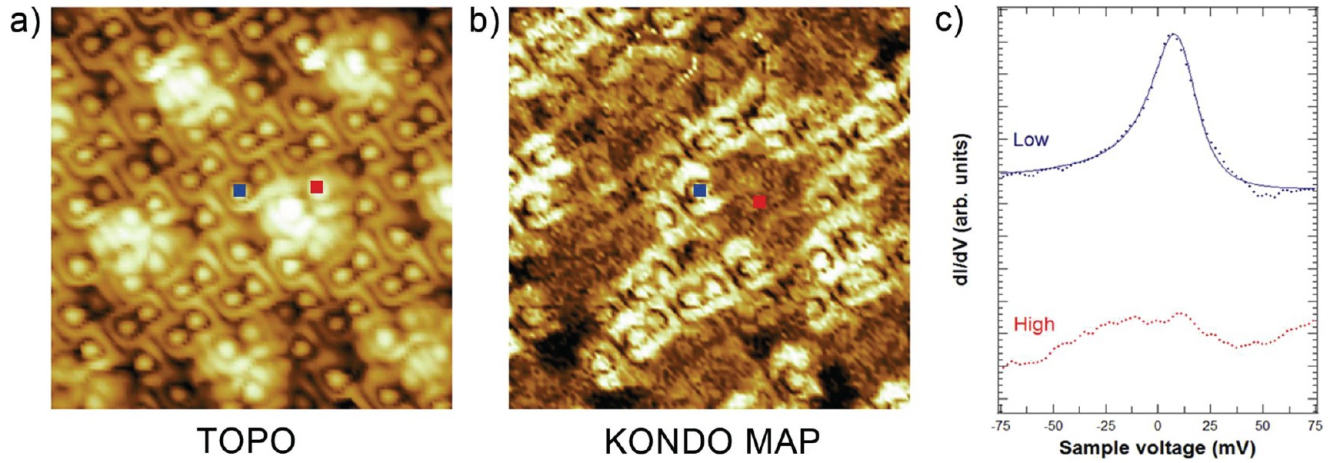

Figure 11. a) Topographic STM image (7 nm × 7 nm) of a monolayer of TCNQ/gr/Ru(0001) recorded at 4.6 K with a sample voltage of 100 mV and a tunnel current of 20 pA. The molecules at the upper part of the ripples appear bright; b) Spectroscopic dI/dV (x,y) map at −0.1 meV recorded simultaneously with the STM image showing the spatial distribution of the Kondo resonance at the Fermi level. c) High resolution tunnel spectra recorded on top of TCNQ molecules adsorbed on the valleys (low, in blue) and on the upper part of the ripples (high, in red). Notice that the Kondo resonance is only detected on the lower part of the ripples.

by the gr/Ru(0001) and generate the associated long-range magnetic order.

The existence of magnetic moments related to the unpaired electrons transferred to the TCNQ molecules can be demonstrated by visualizing the related Kondo resonance.[39] The shielding of a magnetic impurity by the conduction electrons generates a many body electron state that, in turn, originates a narrow resonance at the Fermi level at temperatures below a characteristic Kondo temperature, T_K. High resolution local tunnel spectroscopy at low temperature can reveal this narrow resonance.[41] The local differential conductance spectra reproduced in the right panel of Figure 11 show that the TCNQ molecules adsorbed on the lower part of the ripples, i.e. those charged, do present indeed a magnetic moment, as proven by the appearance of a sharp, narrow resonance at the Fermi level. On the contrary, the uncharged molecules adsorbed on the upper part of the ripples do not display the resonance at the Fermi level. The resonance observed on the TCNQ molecules in the valleys follows the expected temperature dependence for a Kondo resonance.[42] The evolution of the energy width of the resonance with the temperature can be fitted to $2\Gamma = [(\alpha k_B T)^2 + (2k_B T_K)^2]^{1/2}$ and yields Kondo temperatures of T_K = 66 K−139 K depending on the specific adsorption site (fcc-top or bridge) in the valleys. The spatial mapping of the intensity of the Kondo resonance shown in the center panel of Figure 11 visualizes that the uncharged molecules adsorbed on the hills do not possess magnetic moment.

CONCLUSION

In summary, TCNQ molecules deposited on the rippled gr/Ru(0001) display a charged species adsorbed on the lower parts of the ripples and a neutral species adsorbed on the upper part of the hills. The charged species has an associated magnetic moment which is absent for the neutral molecules adsorbed on the upper part of the ripples. On the contrary, TCNQ adsorbed on gr/Ir(111) is not charged and do not present magnetic properties.

EXPERIMENTAL SECTION

Sample Preparation. The experiments were performed in two Ultra High Vacuum (UHV) chambers with base pressures of 3×10^{-11} Torr. The first one was also used to grow and characterize the graphene monolayers on Ru(0001) and Ir(111) by STM. The second one was equipped with XPS/UPS and Organic Molecular Beam Epitaxy (OMBE) sources for molecular deposition.

The Ru(0001) and Ir(111) samples were covered with a single layer of epitaxial graphene by exposing the crystals to a low pressure of ethylene at 1200 K followed by a flash to 1400 K. The graphene covered samples were transferred to the OMBE/XPS chamber and cleaned there by annealing in UHV at 1000 K during 2 min. After that, only a very small amount of oxygen was found by XPS. It was due to some residual patches of the metal surface not covered with graphene prior to the transfer. The intact nature of the graphene overlayer was confirmed by the observation of the characteristic moiré patterns for periodically rippled graphene/Ru[10,13−15] and graphene/Ir[11] by means of Low Energy Electron Diffraction (LEED).

In both chambers the TCNQ molecules were sublimated at 350 K from quartz crucibles with temperature control heated by a tungsten filament. The samples were held at room temperature (RT) during the deposition but cooled down to 4.6 K for imaging.

STM/STS. The variable temperature STM has been described before.[10] The local spectroscopy measurements were carried out at 4.6 K with a low Temperature Microscope using UHV-cleaned tungsten tips as described in ref 43. All the STM data have been analyzed with WSxM software.[44]

XPS Measurements. The second UHV chamber was equipped with an Organic Molecular Beam Epitaxy (OMBE) system, a monochromatized X-ray source, an ultraviolet He discharge lamp, a hemispherical energy analyzer (SPHERA-U7), and a low energy electron diffraction (LEED) optics. The unpolarized He I ($h\nu$ = 21.2 eV) and He II ($h\nu$ = 40.8 eV) lines of the UV lamp were used for Ultraviolet Photoelectron Spectroscopy (UPS), and the Al Kα line ($h\nu$ = 1486.7 eV) was used from an Al anode for X-ray Photoelectron Spectroscopy (XPS). The analyzer pass energy was set to 20 eV for the XPS measurements to have a resolution of 0.6 eV, whereas for the UPS the pass energy was set to 5 eV corresponding to a resolution of 0.1 eV. The angular acceptance for the used aperture size is defined solely by the magnification mode, i.e. 1750 × 2750 μm^2. The core level spectra were fitted to mixed Gaussian−Lorentzian components using XPS CASA software; all the binding energies are referred to the sample Fermi level.

dx.doi.org/10.1021/cm5005467 | Chem. Mater. XXXX, XXX, XXX−XXX

AUTHOR INFORMATION

Corresponding Author

*E-mail: rodolfo.miranda@imdea.org.

Notes

The authors declare no competing financial interest.

ACKNOWLEDGMENTS

Financial support from projects CONSOLIDER on Molecular Nanoscience, FIS-2010-15127, FIS-2010-18847, MAT-2012-39308, MAT2011-25598, and Nanobiomagnet is gratefully acknowledged.

REFERENCES

(1) Himpsel, F. J.; Ortega, J. E.; Mankey, G. J.; Willis, R. F. *Adv. Phys.* **1998**, *47*, 511−597.

(2) Martín, J.; Nogues, J.; Liu, K.; Vicent, J.; Schuller, I. K. *J. Magn. Magn. Mater.* **2003**, *256*, 449−501.

(3) Barth, J. V.; Costantini, G.; Kern, K. *Nature* **2005**, *437*, 671−679.

(4) Hu, Z.; Li, B.; Zhao, A.; Yang, J.; Hou, J. G. *J Phys. Chem. C* **2008**, *112*, 13650−13655.

(5) Miller, J. S.; Calabrese, J. C.; Rommelmann, H.; Chittipeddi, S. R.; Zhang, J. H.; Reiff, W. M.; Epstein, A. J. *J. Am. Chem. Soc.* **1987**, *109*, 769−781. Chittipeddi, S.; Cromack, K. R.; Miller, J. S.; Epstein, A. J. *Phys. Rev. Lett.* **1987**, *58*, 2695−2698.

(6) Manriquez, J. M.; Yee, G. T.; Mclean, R. S.; Epstein, A. J.; Miller, J. S. *Science* **1991**, *252*, 1415−1417.

(7) Miller, J. S.; Epstein, A. J. *Angew. Chem., Int. Ed.* **1994**, *33*, 385−415.

(8) Blundell, S. J.; Pratt, F. L. *J. Phys: Condens. Matter* **2004**, *16*, R771.

(9) Garnica, M.; Stradi, D.; Barja, S.; Calleja, F.; Diaz, C.; Alcami, M.; Martin, N.; Vazquez de Parga, A. L.; Martin, F.; Miranda, R. *Nat. Phys.* **2013**, *9*, 368−374.

(10) Vázquez de Parga, A. L.; Calleja, F.; Borca, B.; Passeggi, M. C. G.; Hinarejos, J. J.; Guinea, F.; Miranda, R. *Phys. Rev. Lett.* **2008**, *100*, 056807.

(11) Coraux, J.; N'Diaye, A. T.; Busse, C.; Michely, T. *Nano Lett.* **2008**, *8*, 565−570. N'Diaye, A. T.; Coraux, J.; Plasa, T. N.; Busse, C.; Michely, T. *New J. Phys.* **2008**, *10*, 043033.

(12) Pletikosić, I.; Kralj, M.; Pervan, P.; Brako, R.; Coraux, J.; N'Diaye, A. T.; Busse, C.; Michely, T. *Phys. Rev. Lett.* **2009**, *102*, 056808.

(13) Martoccia, D.; Bjorck, M.; Schleputz, C. M.; Brugger, T.; Pauli, S. A.; Patterson, B. D.; Greber, T.; Willmott, P. R. *New J. Phys.* **2010**, *12*, 043028.

(14) Koch, S.; Stradi, D.; Gnecco, E.; Barja, S.; Kawai, S.; Daz, C.; Alcami, M.; Martin, F.; Vazquez de Parga, A. L.; Miranda, R.; Glatzel, T.; Meyer, E. *ACS Nano* **2013**, *7*, 2927−2934.

(15) Sutter, P.; Flege, J.-I.; Sutter, E. A. *Nat. Mater.* **2008**, *7*, 406−411.

(16) Barja, S. Ph.D. Thesis, Universidad Autónoma de Madrid, 2012.

(17) Borca, B.; Barja, S.; Garnica, M.; Sanchez-Portal, D.; Silkin, V. M.; Chulkov, E. V.; Hermanns, C. F.; Hinarejos, J. J.; Vazquez de Parga, A. L.; Arnau, A.; Echenique, P. M.; Miranda, R. *Phys. Rev. Lett.* **2010**, *105*, 036804.

(18) Stradi, D.; Barja, S.; Diaz, C.; Garnica, M.; Borca, B.; Hinarejos, J. J.; Sanchez-Portal, D.; Alcami, M.; Arnau, A.; Vazquez de Parga, A. L.; Miranda, R.; Martin, F. *Phys. Rev. Lett.* **2011**, *106*, 186102.

(19) Stradi, D.; Barja, S.; Diaz, C.; Garnica, M.; Borca, B.; Hinarejos, J. J.; Sanchez-Portal, D.; Alcami, M.; Arnau, A.; Vazquez de Parga, A. L.; Miranda, R.; Martin, F. *Phys. Rev. B* **2012**, *85*, 121404.

(20) Castellanos-Gómez, A.; Rubio-Bollinger, G.; Barja, S.; Garnica, M.; Vazquez de Parga, A. L.; Miranda, R.; Agrait, N. *Appl. Phys. Lett.* **2013**, *102*, 063114.

(21) Barja, S.; Garnica, M.; Hinarejos, J. J.; Vazquez de Parga, A. L.; Martin, N.; Miranda, R. *Chem. Commun.* **2010**, *46*, 8198−8200.

(22) Hamalainen, S. K.; Stepanova, M.; Drost, R.; Liljeroth, P.; Lahtinen, J.; Sainio, J. *J. Phys. Chem. C* **2012**, *116*, 20433−20437.

(23) Lindquist, J. M.; Hemminger, J. C. *J. Phys. Chem.* **1988**, *92*, 1394−1396.

(24) Higo, M.; Futagawa, T.; Mitsushio, M.; Yoshidome, T.; Ozono, Y. *J. Phys. Chem. B* **2003**, *107*, 5871−5876.

(25) Tseng, T.-C.; et al. *Nat. Chem.* **2010**, *2*, 374−379.

(26) Coletti, C.; Riedl, C.; Lee, D. S.; Krauss, B.; Patthey, L.; von Klitzing, K.; Smet, J. H.; Starke, U. *Phys. Rev. B* **2010**, *81*, 235401.

(27) Preobrajenski, A. B.; Ng, M. L.; Vinogradov, A. S.; Martensson, N. *Phys. Rev. B* **2008**, *78*, 073401.

(28) Grobman, W. D.; Pollak, R. A.; Eastman, D. E.; Maas, E. T.; Scott, B. A. *Phys. Rev. Lett.* **1974**, *32*, 534−537.

(29) Lipari, N. O.; Nielsen, P.; Ritsko, J. J.; Epstein, A. J.; Sandman, D. J. *Phys. Rev. B* **1976**, *14*, 2229−2238.

(30) Medjanik, K.; Perkert, S.; Naghavi, S.; Rudloff, M.; Solovyeva, V.; Chercka, D.; Huth, M.; Nepijko, S. A.; Methfessel, T.; Felser, C.; Baumgarten, M.; Müllen, K.; Elmers, H. J.; Schönhense, G. *Phys. Rev. B* **2010**, *82*, 245419.

(31) Kanai, K.; Akaike, K.; Koyasu, K.; Sakai, K.; Nishi, T.; Kamizuru, Y.; Nishi, T.; Ouchi, Y.; Seki, K. *Appl. Phys. A: Mater. Sci. Process.* **2009**, *95*, 309−313.

(32) Torrente, I. F.; Franke, K. J.; Pascual, J. I. *Int. J. Mass Spectrom.* **2008**, *277*, 269−273.

(33) Scardamaglia, M.; Lisi, S.; Lizzit, S.; Baraldi, A.; Larciprete, R.; Mariani, C.; Betti, M. G. *J. Phys. Chem. C* **2013**, *117*, 3019−3027.

(34) Zhang, H. G.; Sun, J. T.; Low, T.; Zhang, L. Z.; Pan, Y.; Liu, Q.; Mao, J. H.; Zhou, H. T.; Guo, H. M.; Du, S. X.; Guinea, F.; Gao, H.-J. *Phys. Rev. B* **2011**, *84*, 245436.

(35) Yang, K.; Xiao, W. D.; Jiang, Y. H.; Zhang, H. G.; Liu, L. W.; Mao, J. H.; Zhou, H. T.; Du, S. X.; Gao, H.-J. *J. Phys. Chem. C* **2012**, *116*, 14052−14056.

(36) Lu, J.; Yeo, P. S. E.; Zheng, Y.; Yang, Z.; Bao, Q.; Gan, C. K.; Loh, K. P. *ACS Nano* **2012**, *6*, 944−950.

(37) Wackerlin, C.; Iacovita, C.; Chylarecka, D.; Fesser, P.; Jung, T. A.; Ballav, N. *Chem. Commun.* **2011**, *47*, 9146−9148.

(38) Redhead, P. *Vacuum* **1962**, *12*, 203−211.

(39) Kondo, J. *Prog. Theor. Phys.* **1964**, *32*, 37−49.

(40) Chen, W.; Qi, D.; Gao, X.; Thye Shen Wee, A. *Prog. Surf. Sci.* **2009**, *84*, 2789−321. Chen, W.; Qi, D.; Gao, X.; Thye Shen Wee, A. *J. Am. Chem. Soc.* **2007**, *129*, 10418.

(41) Madhavan, V.; Chen, W.; Jamneala, T.; Crommie, M. F.; Wingreen, N. S. *Science* **1998**, *280*, 567−569.

(42) Wahl, P.; Diekhöner, L.; Schneider, M. A.; Vitali, L.; Wittich, G.; Kern, K. *Phys. Rev. Lett.* **2004**, *93*, 176603.

(43) Vázquez de Parga, A. L.; Hernan, O. S.; Miranda, R.; Levy Yeyati, A.; Mingo, N.; Martin-Rodero, A.; Flores, F. *Phys. Rev. Lett.* **1998**, *80*, 357−360.

(44) Horcas, I.; Fernández, R.; Gómez-Rodríguez, J. M.; Colchero, J.; Gómez-Herrero, J.; Baró, A. *Rev. Sci. Instrum.* **2007**, *78*, 013705.